Journal of Marine Science and Technology

Volume 24 | Issue 6 Article 18

INSTANTANEOUS SHORELINE MAPPING FROM WORLDVIEW-2 SATELLITE IMAGES BY USING SHADOW ANALYSIS AND SPECTRUM MATCHING TECHNIQUES

I-Chieh Lee
National Central University, Postdoctoral Fellow, Center for Space and Remote Sensing Research, Taoyuan, Taiwan, R.O.C., whitefanglee@gmail.com

Recommended Citation
Lee, I-Chieh (2016) "INSTANTANEOUS SHORELINE MAPPING FROM WORLDVIEW-2 SATELLITE IMAGES BY USING SHADOW ANALYSIS AND SPECTRUM MATCHING TECHNIQUES," *Journal of Marine Science and Technology*: Vol. 24: Iss. 6, Article 18.
DOI: 10.6119/JMST-016-1026-9
Available at: https://jmstt.ntou.edu.tw/journal/vol24/iss6/18

INSTANTANEOUS SHORELINE MAPPING FROM WORLDVIEW-2 SATELLITE IMAGES BY USING SHADOW ANALYSIS AND SPECTRUM MATCHING TECHNIQUES

Acknowledgements

This research was for the most part completed during the author's Ph.D study at Ohio State University under the supervision of Dr. Rongxing Li, and it was funded by the Ohio Sea Grant College Program (R/CE-010). Special gratitude is extended to Dr. Fuan Tsai at National Central University for providing valuable perspectives and suggestions to improve this paper.

Journal of Marine Science and Technology, Vol. 24, No. 6, pp. 1204-1216 (2016)
DOI: 10.6119/JMST-016-1026-9

INSTANTANEOUS SHORELINE MAPPING FROM WORLDVIEW-2 SATELLITE IMAGES BY USING SHADOW ANALYSIS AND SPECTRUM MATCHING TECHNIQUES

I-Chieh Lee

Key words: image analysis, image segmentation, oceanography, remote sensing.

ABSTRACT

Shoreline mapping and monitoring are crucial in heavily eroding coastal areas. Frequently monitoring shoreline changes in eroding areas can help government agencies to understand the causes and formulate plans to protect the shoreline; however, the cost of data sources and human labor involved can be prohibitive. To address this problem, this research proposes a cost-effective and semiautomatic shoreline delineation procedure that uses WorldView-2 satellite images as the data source. The advantages of the proposed procedure are the use of shadow and spectrum information, as well as the application of object-oriented classification. The classification process incorporates new bands from WorldView-2 to perform spectrum analysis on multispectral images; subsequently, a new pan-transferring process for the classification result is proposed to maximize the resolution. Finally, a classification adjustment process based on scenario analysis using shadows as information is applied. This procedure remedies the problems caused by shadow areas and converts them into elevation information to minimize errors in shoreline delineation. The analysis results indicate that the proposed procedure can derive the location of an instantaneous shoreline with an accuracy of 1.8 m (root-mean-square error) in a test area of Painesville, Ohio, USA.

I. INTRODUCTION

Shoreline mapping has been a labor-intensive and time- and cost-consuming process since the ground survey era until the recent aerial photogrammetry era (Shalowitz, 1964; White, 2007), and these obstacles have effectively prevented frequent shoreline mapping. Significant shoreline erosion has occurred along the southern shore of Lake Erie, Ohio, and bluffline erosion has reached 1.8 m/yr in the region of Painesville (Srivastava, 2005). Shorelines must be frequently measured to derive the cause of the erosion and formulate plans to prevent further erosion. Recently, researchers have proposed new shoreline mapping procedures that entail adopting new equipment and data including satellite images (Di et al., 2003; Li et al., 2003; Scott et al., 2003; Liu and Jezek, 2004) and aerial laser scanning (ALS) systems (Li et al., 2002; Stockdon et al., 2002; Robertson et al., 2004; Liu et al., 2009; White et al., 2011) to reduce the cost of data sources and human labor. If cost is the main concern, satellite images could be the most cost-effective data source for shoreline mapping compared with ground survey, aerial photogrammetry, and ALS systems, because the level of human labor required is significantly lower.

Most studies on shoreline delineation from satellite imagery are based on supervised classification algorithms (Sekovski et al., 2014). In such algorithms, indicators (features) are selected, such as the normalized difference vegetation index (NDVI) or normalized difference water index (NDWI), followed by the execution of the training and classification procedures. After classification, accuracy assessment statistics are provided. In this study, we executed shoreline delineation from a different prospective. Two goals were established for developing a new shoreline delineation algorithm: First, we classified everything apart from water because of the noisiness of water surfaces on a satellite image. Second, we developed an algorithm that, as far as possible, does not require a training process; that is, we developed an algorithm with fully autonomous potential.

Herein, we present a shoreline delineation procedure for extracting instantaneous shorelines from WorldView-2 satellite images. Because acquiring satellite imagery at an exact location at an exact time is nearly impossible, the shoreline depicted in satellite images represents the shoreline at the time of imaging, and it does not correspond to any tide-coordinated water levels; therefore, shorelines delineated from satellite images can only be treated as instantaneous shorelines (Li et al., 2002; Boak and Turner, 2005). The proposed shoreline delineation

Paper submitted 05/27/16; revised 06/16/16; accepted 11/15/16. *Author for correspondence: I-Chieh Lee (e-mail: whitefanglee@gmail.com).*
National Central University, Postdoctoral Fellow, Center for Space and Remote Sensing Research, Taoyuan, Taiwan, R.O.C.

procedure incorporates shadow analysis, a pan-transferring classification process for achieving a higher degree of automation, relatively low costs for data source acquisition, and improved accuracy of delineated shorelines.

II. BACKGROUND

1. Shoreline Detection within Shadow Areas

The existence of shadows in aerial photographs and satellite images is an inevitable inconvenience during feature classifications and localizations. Shadows may exist at any location that has an elevation difference, and shadow directions vary by the time of the day and seasons; these phenomena not only increase the difficulty for computer algorithms to delineate shorelines but also complicate determining shoreline locations manually. Most shoreline extraction research has largely ignored shadow areas, and even when addressed, the method applied entailed manual delineation (Di et al., 2003).

In the current study, we selected Painesville, Ohio, located on the southern shore of Lake Erie, approximately 41°N, as the study area. Because the sun angle is lower at higher latitudes even at noon, obstacles along the southern shore (e.g., trees, buildings, and coastal man-made structures) project a shadow onto the water surface. The worst-case scenario is the boundary between land and the water surface being in the shade, masking the shoreline. Even if some areas of the shoreline can be slightly delineated, the result is not reliable. Because many shadow areas are likely caused by man-made structures, these clues can be incorporated into the satellite image classification process to help determine the class of the shadow and surrounding areas. Shadows have previously been treated as an obstacle in remote sensing classification (Yamazaki et al., 2009); however, in this research, we treated them as a source of information providing elevation differences to minimize the impact caused by shadow areas in shoreline delineation.

2. Features of WorldView-2

WorldView-2 is one of the latest remote sensing satellites operated by DigitalGlobe. The difference between WorldView-2 and the previous Quickbird satellite is not only the improvement in spatial resolution but also the increase in the spectral resolution to cover additional multispectral bands. WorldView-2 has one panchromatic band and eight multispectral bands (Coastal Blue, Blue, Green, Yellow, Red, Red Edge, N-IR 1, and N-IR 2); the spatial resolution is 2.0 m in the multispectral bands and has been improved from 0.7 m (Quickbird) to 0.5 m (WorldView-2) in the panchromatic band. The point positioning accuracy without ground control points has also been improved from 23 m (Quickbird) to 6.5 m (WorldView-2) (DigitalGlobe, 2013). In this research, we incorporated the new bands into the classification and demonstrated the use of their advanced features.

3. Definition of Shoreline

From a typical aerial photograph, multiple linear features can be observed along a coastline (Fig. 1) that are caused by man-made structures, water lines, wave fronts, breaking waves, and other objects. Although delineating instantaneous shorelines was the primary objective of this study, we must also determine which linear features to examine and map.

Fig. 1. Linear features along the land-water interaction zone. (Credit: Bing Map).

In the United States, the legal shorelines are tide-coordinated shorelines defined by the National Oceanic and Atmospheric Administration (NOAA) and recognized by the US Federal Geographic Data Committee. The mean high water (MHW) line in tidal areas and the mean water level line in nontidal areas are examples of these legally recognized shorelines (Hicks and Schureman, 2000). The National Geodetic Survey (NGS) at NOAA is the agency responsible for mapping and managing the US legal shoreline, and its guidelines form the definition used in this research to determine shoreline location. The NGS roughly classifies shorelines into four types: (1) engineered shoreline, (2) lines for which the water does not intersect with dry ground (e.g., marshes or glaciers), (3) lines in nontidal areas, and (4) lines in tidal areas (Leigh, 2012). Because of the properties of the shoreline in the study area, this study considered only the definitions for engineered shorelines and nontidal areas. The extracted shoreline is an instantaneous shoreline, instead of a tide-coordinated shoreline.

Legal shorelines in the United States are delineated mainly from the stereoscopic environment of aerial photogrammetric procedures described by the NGS (White, 2007). The identification of the MHW line on an aerial photograph involves using closely correlated physical evidence such as berms and debris lines, wet-dry sand abutments (tone and texture), or wave action, and is subject to human interpretation (White, 2007; Leigh, 2012). Because satellite imagery was the only data source in this research, detecting the elevation difference of berms was impractical; hence, the tone and texture differences of the wet-dry sand abutment created by the last run-up wave (the instantaneous water line indicated in Fig. 1) were used to identify the shorelines in sediment bank and sloped structure areas.

III. METHODOLOGY

The concept of the proposed instantaneous shoreline extraction procedure is to classify a satellite image and then trace the boundary of the classes belonging to a land class (Fig. 2). In

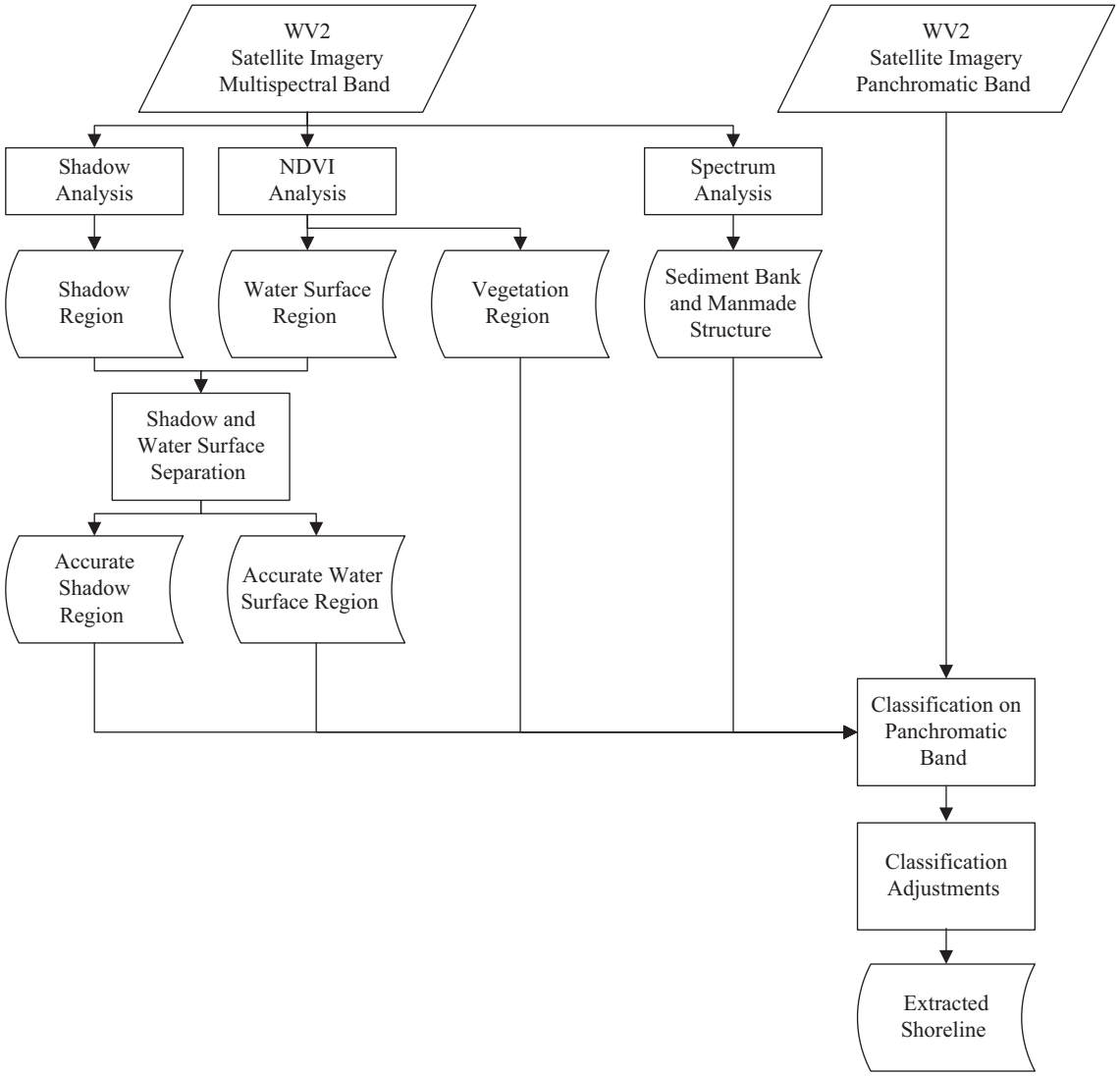

Fig. 2. General procedure of instantaneous shoreline delineation from a WorldView-2 image.

the classification stage, knowledge-based classification methods are used to classify multispectral satellite image pixels into four categories: shadow, water surface, vegetation, and sediment bank/man-made structure. The proposed classification process modifies well-known and proven algorithms and indices, the NDVI and spectrum matching, to preliminarily classify images into one of the four categories.

The proposed methods emphasize shadow area analysis and determining the water-land separation within unclassified areas. First, areas within a shadow could either be the water surface or land class. After the analysis of the on-site topology of how the shadow areas are created within the coastal area, rules can be established to minimize the shoreline delineation error created by shadow areas. Next, through the use of image resampling, image segmentation, and classification stacking processes, the classification result of the multispectral bands are assigned to the panchromatic image to fully utilize the higher resolution provided by WorldView-2. Unclassified areas in the preliminary classification result must be assigned to the land or water surface class by analyzing the possible terrain by using the surrounding classifications. After the classification process, the separation between the water and land classes is extracted to determine the location of the shorelines.

1. Shadow Areas, Water Surfaces, and Vegetation Areas

The water surface class is the key class for extracting the shorelines, but other classes are necessary for fine-tuning the separation between water and land. Detecting water surfaces from multispectral satellite imagery has been widely studied in the remote sensing field. Indices such as the NDWI, modified NDWI, and normalized difference pond index are basically modifications of the NDVI. These indices were modified to accommodate different data sources and different applications (Ji et al., 2009). In this research, each of these indices was tested, and the results showed no significant advantage compared with the NDVI for the data sources used; hence, the NDVI was

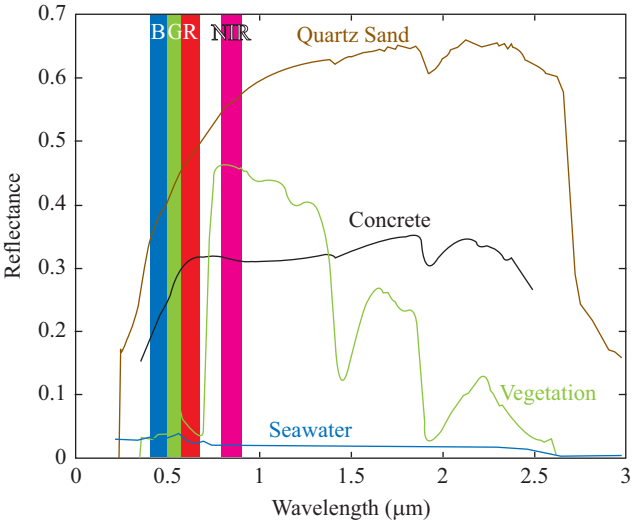

Fig. 3. Spectral plot of the four major objects in the study area (Modified from USGS spectral library).

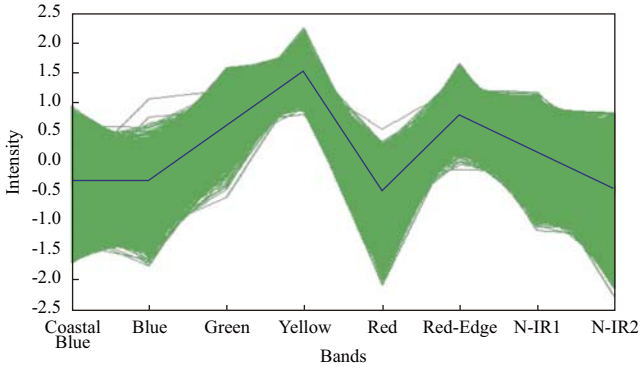

Fig. 4. Plots of normalized intensities of manually selected sandy beach samples with the mean value represented by the blue line.

adopted to classify water surfaces and vegetation areas.

The exact threshold for the water surface and vegetation classes was determined through a trial-and-error process. An empirical threshold was given as an initial value, the classification result manually studied, and the threshold adjusted until all significant features were classified correctly. Thus, vegetation was defined as areas with NDVI values higher than the threshold of 0.55 and water surfaces as areas with NDVI values lower than the threshold of -0.1.

After this process, the water surface and vegetation classes were classified; however, water surface areas are easily mixed with shadow areas, especially calm water surfaces, because of the similarity in the reflectance of water surface and shadow areas on the red and NIR bands and similarity in the NDVI values of these areas (water surface is near zero to slightly negative, and shadow areas are around zero). Because accurately segmenting the water surface region is the only means of obtaining an accurate shoreline, an algorithm that can separate these regions effectively must be developed; thus, an additional procedure is required to separate the water surface class from shadow areas.

Shadows are caused by natural and man-made objects close to the shoreline; hence their intensity values across all multispectral bands are uniformly lower. By contrast, water surface intensity values can be relatively high in some electromagnetic bands but low in others; this is because water absorbs sunlight, and the absorption rate differs across different electromagnetic bands. The water surface reflectance was higher, between 500 and 600 nm (Fig. 3), a bandwidth of electromagnetic wave that corresponds to the green and yellow bands in WorldView-2. An inspection of the water surface intensity values in the satellite image areas indicated that they were significantly higher in the green and yellow bands—approximately 100 intensity units higher than that of the shadows on both bands.

On the basis of the previous observation, a solution was developed to sum the green and yellow bands and determine the intensity value threshold manually by selecting a relatively large shadow area and finding the maximum intensity value within the shadow area. The intensity value of the shadow pixels must not be mixed with the intensity value of the water surface. Summing the intensity values of the green and yellow bands by using current data sources revealed that the manually determined intensity threshold was 350 intensity units.

2. Sediment Bank/Man-Made Structures

Although the WorldView-2 satellite is equipped with an eight-band multispectral sensor, the spectral resolution is insufficient for classifying every object in an image. During the design phase of this research, we assumed that the sediment bank and man-made structures could be separated into two classes; however, after performing separability tests, we realized that they could not be separated with the data source used. Regarding material composition, silicon is the major compound in both the sediment bank and man-made structures; hence, the fact that these two objects cannot be separated by physical properties is reasonable. The spectral reflectance curve (Fig. 3) shows that the sediment bank and man-made structures are significantly different from other classes and should be easily separated; hence, a procedure similar to the spectrum-matching approach used in hyperspectral image classification was implemented to classify sediment bank/man-made structure areas.

For classifying the sediment bank/man-made structures, we first manually selected a set of sandy beach pixels and retrieved the intensity value for each band. We then calculated the mean and standard deviation of the intensities from all bands and used them as shifting and scaling parameters to analyze the significant relationships of intensity between each band (Fig. 4). The blue line in Fig. 4 represents the created criteria, which denote the average normalized intensity of each band. The description of the criteria is listed:

- $I_{Yellow} > I_{Green}$
- $I_{Green} > I_{Blue}$; $I_{Green} > I_{Coastal\text{-}Blue}$
- $I_{Yellow} > I_{Red\text{-}Edge} > I_{NIR\text{-}1} > I_{NIR\text{-}2}$

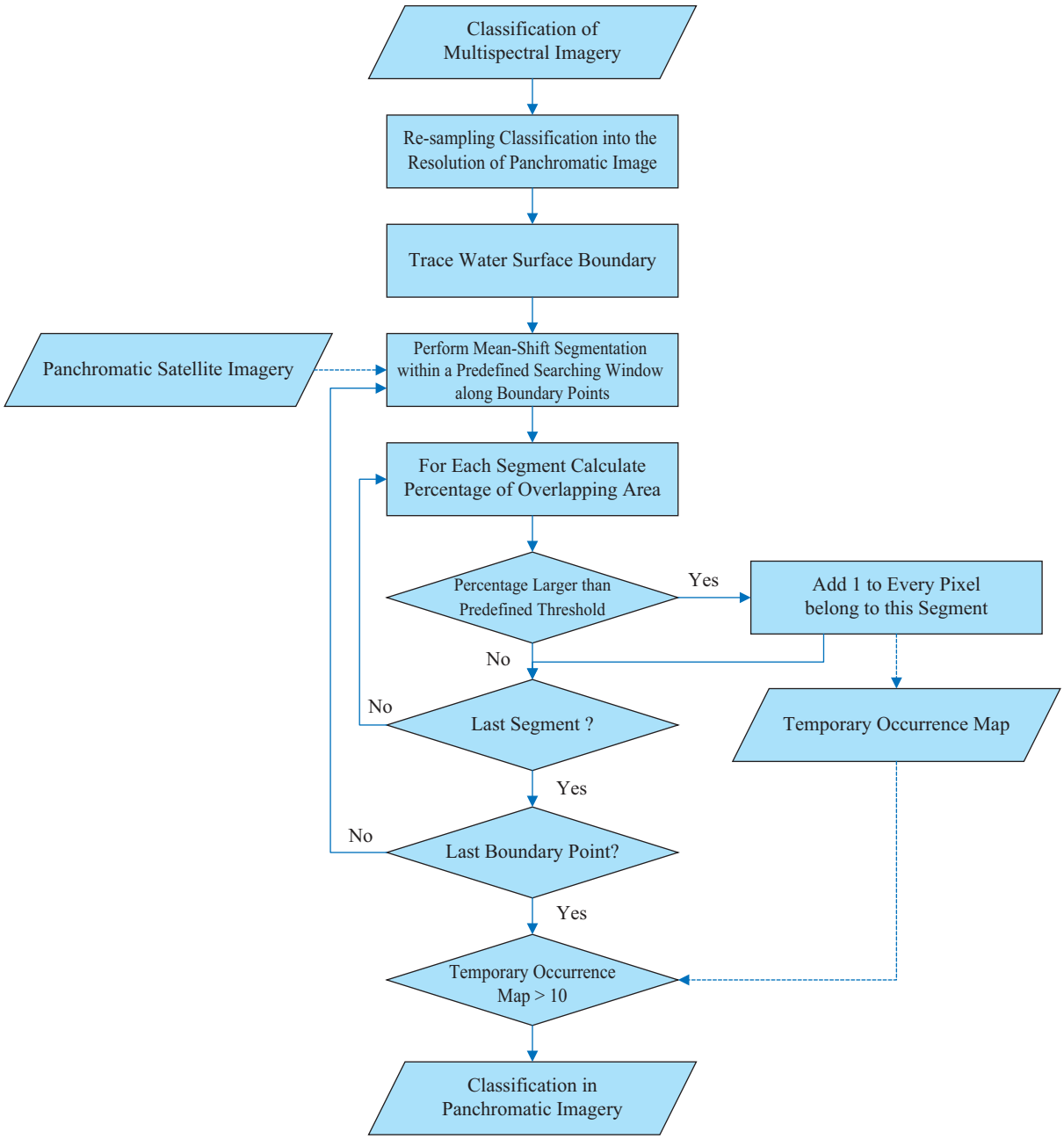

Fig. 5. Flowchart of transferring multispectral band classification results onto the panchromatic band.

- $I_{NIR\text{-}1} > I_{Red}$
- $I_{Red\text{-}Edge} > I_{Coastal\text{-}Blue}$

I represents the intensity of the band in subscript. Any pixels in the image satisfying these criteria would be classified as sand.

After the spectrum matching, several types of objects were selected, including sediment banks, concrete surfaces, sand piles, and partial concrete blocks (riprap revetments).

3. Refinement of Classification Results

After the completion of the previous classification processes, four multispectral image classes were identified. Because the resolution of the multispectral imagery is 2 m and that of panchromatic imagery is 0.5 m, the land–water separation must be delineated using the panchromatic image to maximize the accuracy of the extracted shoreline. Hence, the objective of this process is to assign the classification result derived from the multispectral image to the panchromatic image. The traditional pan-sharpening process creates a high-resolution color image (the same resolution as the panchromatic image) by combining the higher-resolution panchromatic and lower-resolution multispectral image (Padwick et al., 2010), a process mainly targeted at producing visually pleasing color images. Because the goal of the current study was to produce a multispectral

image to perform classification, having a spectrally accurate pan-sharpened multispectral image is a major concern. After several trial runs with the WorldView-2 pan-sharpened image, we determined that we must develop a procedure specific to this research that can transfer the classification result onto the panchromatic band. We named such a procedure the pan-transferring process.

To develop this pan-transferring procedure, the original multispectral imagery was used to perform the classification. The identified classes were then resampled from the lower-resolution multispectral imagery to the higher-resolution panchromatic imagery. The four classes identified in the previous processes were used to perform the following process iteratively (Fig. 5): (1) The classification result was resampled to the same resolution as the panchromatic image. (2) The boundary of the water surface class in the resampled classification image was traced to outline a buffer zone representing the coastal area because only the classification within the coastal area was needed. The boundary points on the edge of the satellite image were excluded because they do not belong to the approximate shoreline. (3) A patch of the panchromatic image was cropped out by a search window with a predefined size. (4) Mean-shift segmentation was then applied to this patch. (5) Each class was overlapped onto every segment in the search window to calculate the percentage of overlapping area. (6) A temporary occurrence map that was the size of the panchromatic image was created, with zero being assigned to all elements. For every element of a segment with a percentage of overlap higher than the threshold (the parameter segment overlap percentage, SOP), its corresponding elements on the temporary occurrence map were increased by one. (7) After all segments in the search window were processed, the next water surface boundary point and its corresponding search window were examined until every boundary point was processed and segmented. (8) After all boundary points were processed, the value of each element in the temporary occurrence map represented the number of times that pixel was assigned to a certain class, with higher values representing a more robust assignment of classes. To overcome the noise in each segmentation result, elements with a value < 10 in the temporary occurrence map were reset to zero. In other words, all indices > 10 are the pixels assigned to the class currently being processed. (9) The next class was then processed until all four classes were transferred onto the panchromatic band.

The memory usage and computation time for segmenting the entire satellite image of the study area were not practical for our currently available computer. The described pan-transferring procedure (Fig. 5) was designed to prevent the problem of insufficient computer memory while maintaining a practical computation time. Mean-shift theory is based on a density-driven concept (Fukunaga and Hostetler, 1975); therefore, dividing the image into several sections would conflict with this concept. If the image is divided, the density estimate of the edges of the divided image would not be continuous; hence, the summed occurrences act as a smoothing filter to overcome this drawback. The proposed procedure maintains a manageable memory usage and computation time by reducing the area to be processed and segments the panchromatic image patch by patch while maintaining the density-driven concept of the mean-shift algorithm.

In this study, we incorporated EDISON, an implementation of the mean-shift image segmentation algorithm introduced by Comaniciu and Meer (2002), to perform the image segmentation for each image patch. Each of the four classes had three parameters in the pan-transferring process: one, namely the SOP, from the previously described sequence (item 6); and two, namely the spatial bandwidth and color bandwidth, from the mean-shift image segmentation algorithm. These parameters were determined by following a supervised training process. First, we selected a small training area with multiple terrain types. Second, we manually delineated the ground truth shoreline by following previously described shoreline identification guidelines. Third, we systematically evaluated the shoreline accuracy while adjusting the parameters.

Because the image segmentation was performed separately, discrepancies were observed between classes; such discrepancies involved classes overlapping with one another, and they were caused by the use of different pan-transferring parameters for each class. The goal of the proposed classification and pan-transferring procedure was to delineate an accurate shoreline rather than identify an accurate classification; therefore, a buffer zone was allowed for some of the classes, whereas accuracy was preferred for others. Consequently, how to evaluate and finalize the classifications is highly correlated with the physical properties of each class, identification of shoreline location, and the pan-transferring parameters.

The first issue addressed was the physical and imaging properties of the water surface and sediment classes. From the shoreline definition, we chose the most recent wet-dry line of the wave run-up as the shoreline location; hence, some intensity variations must be tolerated to prevent other earlier watermarks from being segmented. If the most recent watermark is not clear, the sediment bank segment may confuse some of the water surfaces or vegetation areas as sediment banks. However, water surfaces are most often incorrectly segmented because of breaking waves and sun glints. Sun glint areas usually occur on calm water surfaces and are usually not concurrent with waves. Regardless of how calm the water is, some wave activity is always present; hence, sun glint areas do not directly contact the shoreline. By contrast, wave fronts are higher in intensity but are surrounded by lower-intensity water surfaces.

The worst-case scenario for this classification is a breaking wave front occurring directly on the shoreline. In this case, the intensity difference is too high for the corresponding areas to be classified in the water surface class, and no parameter adjustment is required; these areas remain unclassified and the correction is made in the classification adjustment section. Therefore, the intensities are relatively uniform for the water surface class, consequently resulting in a robust classification compared with those of the sediment bank class; therefore, the water surface class is overlaid on the sediment bank class. However, vegetation, shadow, and water surface areas are low-

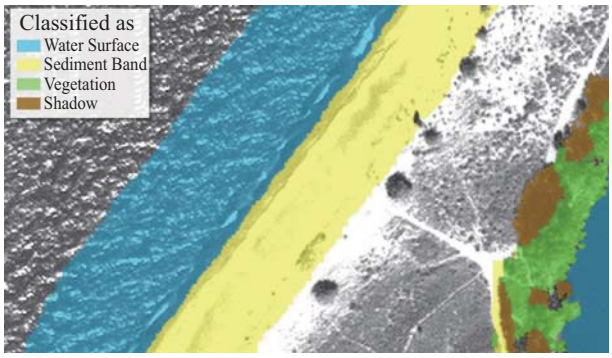

Fig. 6. Ideal water-land intersection for shoreline delineation.

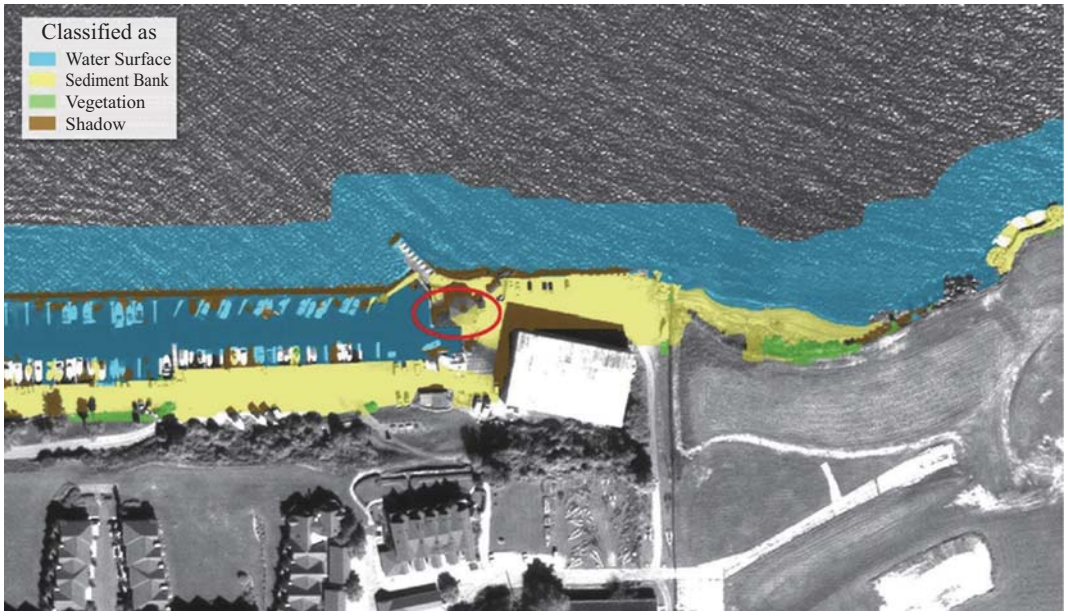

Fig. 8. Shadow was created by the unclassified area; hence, the area was not a water surface area.

intensity features on the panchromatic band. Although vegetation and water surface areas are clearly on opposite sides of the shoreline, the location of shadow areas can be uncertain. The intensity variations of water surface areas are still greater than those of shadow areas, and thus, the segmentation could be relatively robust and accurate in identifying shadow areas. Although the water surface class may occasionally contain segments of vegetation areas because of the parameter settings, the vegetation class would not contain segments of water surface areas. Hence, the vegetation area overlaid with the shadow area to minimize the uncertain areas, and then overlays water surface areas to maintain the most favorable classification results. The stacking sequence is (1) vegetation areas, (2) shadow areas, (3) water surface areas, and (4) sediment banks/man-made structure areas.

4. Classification Adjustment

The best-case scenario of classification for shoreline delineation would be the sediment bank/man-made object class or vegetation class being in immediate proximity to the water surface class (Fig. 6). In this case, the shoreline could be clearly identified as the boundary line of the land; however, this was not always the case after classification. Specifically, unclassified areas would be presented at the edge or next to the water surface, and, because of insufficient information, further identification could only be accomplished using information from other data sources. However, unclassified areas must only be assigned to the land or water surface class. Despite sediment bank/man-made object areas and vegetation areas being clearly classified as land, shadow areas and unclassified areas caused most of the identification problems. All unclassified and shadow areas along the shore must be identified to determine whether they belong to the water surface or the land class.

A rule-based procedure consisting of five rules in three stages (Fig. 7) was developed according to five scenarios that were designed to provide the most accurate shoreline. One rule in the first stage and two rules in the third stage were applied to classify the unclassified areas, and two rules in the

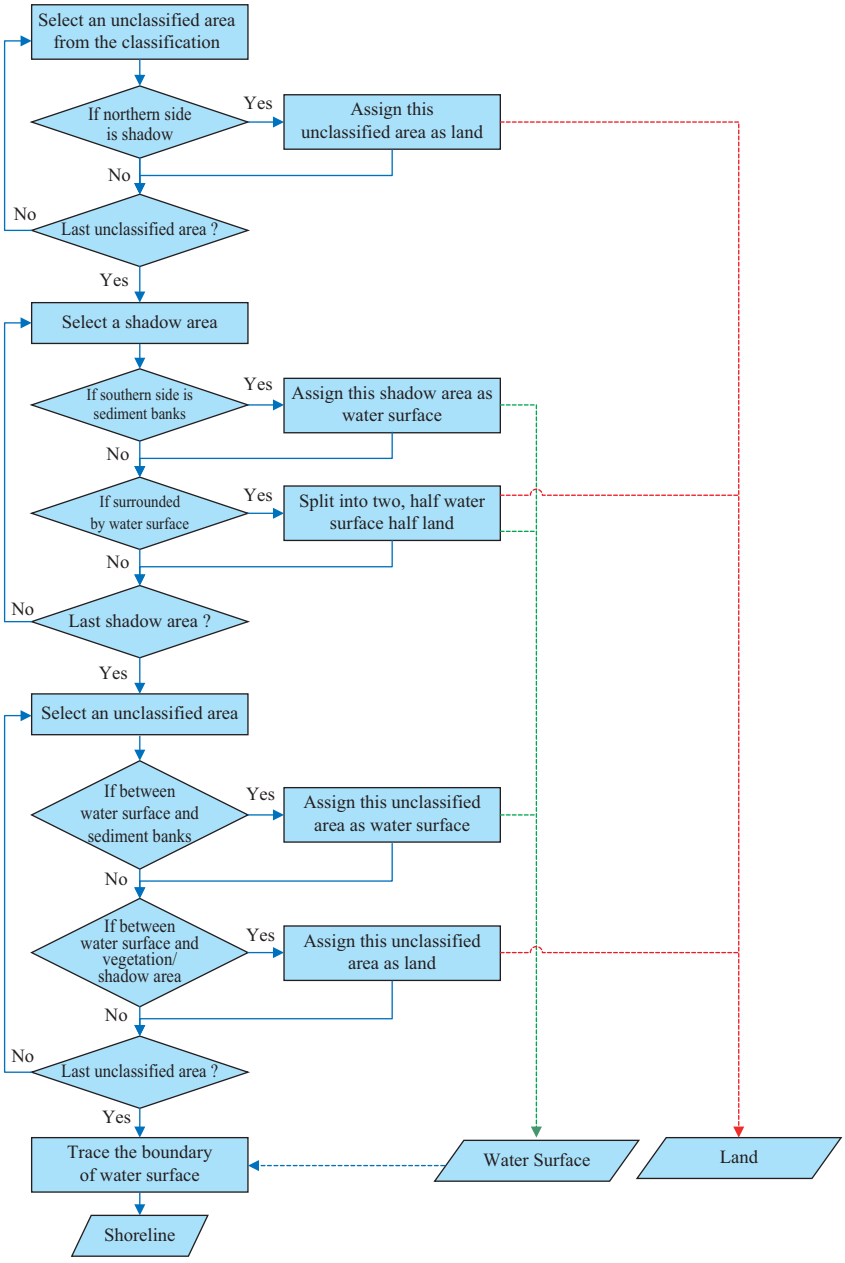

Fig. 7. Flowchart of the classification adjustment process.

second stage were used to classify the shadow areas.

The first rule in the first stage determines if an unclassified class belongs to the land class. Shadows are created in areas in which elevation differences exist between two objects. Because the sun angle within an entire satellite image is uniform, the location of an object with a higher elevation can be determined by the edge of its shadow. Moreover, because the sun angle is due south in the satellite images used in this research, unclassified areas directly in contact with a shadow area to the north represent an object with an elevation higher than that of the shadow area and therefore cannot belong to the water surface class (Fig. 8). Therefore, these unclassified areas are assigned to the sediment bank/man-made object class.

The second stage is to classify the shadow area. Because objects in shadow areas within the study area may be caused by man-made structures, bluff tops, or trees, two rules were applied. The first scenario is that the shadows are created by man-made structures (Fig. 9(a)), and the second scenario is that shadows are created by bluff tops or trees (Fig. 9(b)). If a shadow area created by man-made objects is between the water surface class and sediment bank/man-made object class, and if the southern side (corresponding with the sun angle) belongs to the sediment bank/man-made objects class, this sediment bank/man-made object area can only be a vertical structure or a building. On the basis of the shoreline identification guidelines described previously, this shadow area would be classified as a water surface

(a)

(b)

(c)

Fig. 9. Three types of terrain creating shadow areas. Shadow created by (a) man-made structures, (b) forest (or tree clusters), and (c) trees that can be distinguished individually. (Credit: Bing Map).

area. If the shadows are created by trees or bluff tops, there are three possible scenarios: edge of shadows lying on the land, exactly on the shoreline, or on the water surface (Fig. 10).

If a shadow lies on the land, there should be a sediment bank/man-made object or unclassified class between the shadow and the water surface classes, and no adjustment is required. If the shadow lies exactly on the shoreline or on the water surface, the shadow and the water surface classes are adjacent. The location at which the shadow class and the water surface class meet can be detected, and the location of the shoreline is thus within this shadow area; however, no approach is available for determining whether the boundary is the location of shoreline. Under this circumstance, finding the exact location of the shoreline is impossible; instead, the goal is to find a line that minimizes the shoreline extraction error.

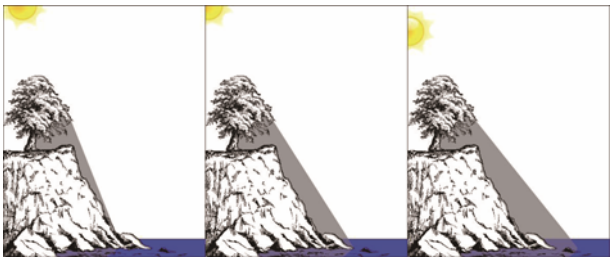

Fig. 10. Possible conditions for a shadow-shoreline relation.

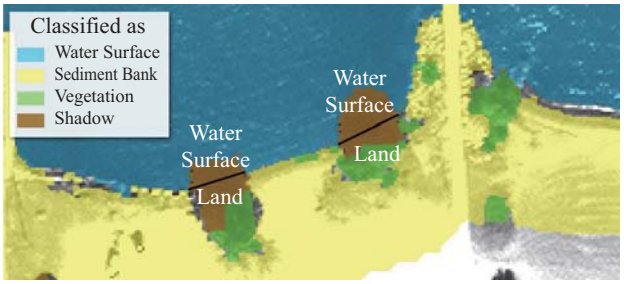

Fig. 11. Shadow area divided into the water surface class and land class based on the surrounding classes.

For long stretches of forest along the shore or bluff (Fig. 9(b)), the shadows created on the water surface are usually spiked or cloud-shaped areas, depending on the shape of the trees forming such shadows. The optimal choice of shoreline estimate would be the polyline connecting the most inward water points within the shadow area. For a single or small cluster of trees (Fig. 9(c)), this could reveal the true classification of this shadow area by the surrounding classes. Therefore, for each shadow area surrounded by water surface and/or other classes, a separation line could be drawn within the shadow area by using the classified neighboring pixels to divide the shadow area into water surface and land classes (Fig. 11). These two shadow scenarios differ in logic but actually share the same processing procedure; both scenarios entail dividing shadow areas by creating a polyline from the surrounding water pixels.

After the completion of the previous stages, the unclassified and shadow classes can be adjusted or reassigned. The third and final stage is to reevaluate the unclassified areas on the basis of the previous adjustments using two rules. First, if unclassified areas are between water surface and sediment bank/man-made object areas, they are assigned as water surface areas because these areas are more likely wet sediment banks on a sandy beach caused by wave run-up (Fig. 12). This condition can also be caused by other situations, such as wet man-made objects; however, if there is no other distinguishing information from the imagery itself, it is accepted as a type two error. Second, if unclassified areas are between or contain sediment bank/man-made object areas, vegetation areas, and/or shadow areas, they are usually sloped structures, namely riprap revetment, and assigned as land (Fig. 13).

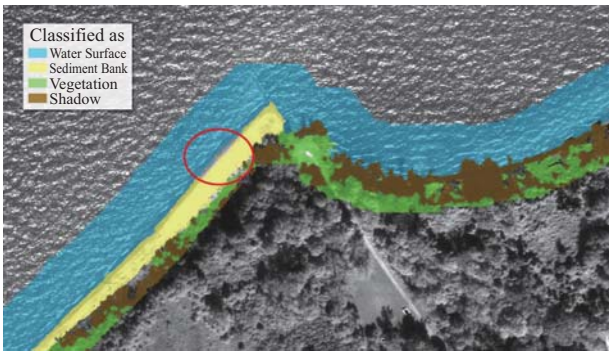

Fig. 12. Unclassified area between the water surface class and the sediment bank. This area usually involves wet sand and should be classified to the water surface class.

Fig. 13. Unclassified area between sediment banks, vegetation areas, and shadow areas.

Fig. 14. WorldView-2 panchromatic band showing the study area: Painesville, Ohio.

After the completion of the process, the classification is adjusted and the critical unclassified areas are assigned. The shoreline can then be delineated by tracing the boundary of the water surface class to create the shoreline extracted from the WorldView-2 satellite imagery.

IV. RESULTS AND DISCUSSION

Our study area, Painesville Township, Ohio, is located 25 miles east of Cleveland, along the southern shore of Lake Erie, in Lake County (Fig. 14). An aerial orthophoto provided by the Ohio Geographically Referenced Information Program (OGRIP) was used to delineate shoreline ground truth. The WorldView-2 satellite image used for this research covered an area 8 km long and 4.5 km wide at UTM 17N and was acquired on September 14, 2010 (16:45 UTC). The package comprised two images: a 0.5-m resolution panchromatic image and a 2.0-m resolution multispectral image with eight bands.

Table 1. Pan-transferring parameters chosen according to the parameter determination guidelines described in Section 3.3. The parameters are color bandwidth (CB), spatial bandwidth (SB), and segment overlap percentage (SOP).

Class	Water Surface	Vegetation	Shadow	Sediment Bank/ Manmade Object
CB	4.5	4.5	5.5	4.5
SB	5	5	5	5
SOP	0.3	0.4	0.5	0.2

To evaluate the accuracy of the extracted shoreline, the ground truth shoreline was delineated manually according to the previously described guidelines based on the panchromatic WorldView-2 satellite imagery and served as a reference line. An aerial orthophoto was used as a secondary data source, in the event that the ground truth shoreline in the grayscale satellite imagery was difficult to determine. The total shoreline length was approximately 14 km, and the terrain types were manually determined while delineating the ground truth. The extracted shoreline was compared against this ground-truthed shoreline by using the method described by Lee et al. (2009).

A set of parameters were selected as presented in Table 1, and shoreline objects were then extracted. The boundary of the water surface class was delineated as an instantaneous shoreline. A statistical analysis was performed (Table 2), revealing that the overall accuracy of the shoreline extracted with this classification result could reach 1.8 m (RMSE, which is less than a pixel of multispectral images). According to the results derived from analyzing the accuracies of the shorelines associated with individual terrain types, the accuracy of the sediment bank areas and groin areas was the highest among all terrain types (0.7 m, slightly larger than one pixel of panchromatic images). Other shoreline objects were extracted with an average error ranging from approximately 1 to 3 m, except piers. The errors were from 1 to 1.5 pixels of the multispectral images used. The average error for piers reached 4.8 m (over 2 pixels) because the anchored vessels were classified as man-made structures.

By comparing the average error and RMSE of each terrain type, we discovered that the RMSE of vertical structures (1.477 m) was significantly higher than the average error (0.839 m). In addition to the high value of the maximum error of the vertical structure areas, these numbers indicate that most components of the shoreline in the vertical structure areas were accurate,

Table 2. Accuracies of the extracted shorelines associated with individual terrain types.

Terrain Type	Length (m)	Maximum Error (m)	Average Error (m)	RMSE (m)
Sediment Bank	3099	7.555	0.665	0.782
Sloped Structure	4822	10.019	1.667	1.673
Vertical Structure	2839	14.540	0.839	1.477
Bluff	1621	7.343	1.703	1.395
Groin	69	1.651	0.660	0.468
Breakwater	96	7.560	2.551	2.058
Shadow	789	10.666	3.041	2.391
Pier	311	11.726	4.766	3.758
Total	13650	14.540	1.464	1.796

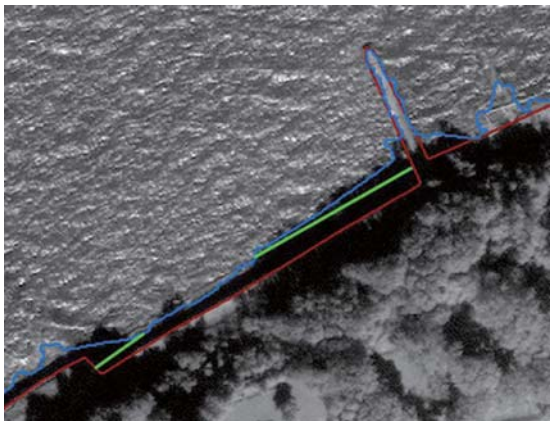

(a)

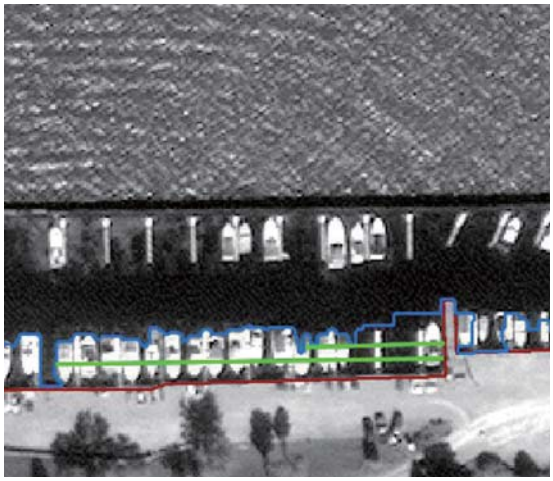

(b)

Fig. 15. Two examples revealing the amplification of the shoreline delineation error by the error estimation method. The red line represents the shoreline ground truth, blue line represents the delineated shoreline, and green line represents the amplified error distance created by the error estimation method.

but some areas had a significant degree of error. These errors were because the imperfect error estimation method amplified the inaccurate shoreline delineation results, particularly in areas with man-made structures. Fig. 15 depicts two examples of shoreline error amplification engendered by the error estimation method. This error amplification problem occurred near the right angle corner of the ground truth shoreline. Apart from manually editing the measurements, no effective solution was available for removing this glitch; hence, we highlight the problem but retain the amplified measurements in our statistics.

After statistical analysis, we analyzed the cause of the inaccuracy of the delineated shoreline by inspecting the in situ data by terrain type. Although the shoreline could be accurately extracted in most of the sediment bank areas (Fig. 16(a)), areas where tone and texture differences were not significant or in proximity to breaking waves could not be extracted as accurately. Significant shoreline delineation errors in areas with sloped structures were engendered by the different materials of riprap revetments (Fig. 16(b)) and by the similarity in panchromatic intensity levels between water surfaces and wet riprap revetments. In the areas with vertical structures, the extracted shoreline was relatively accurate, particularly in areas in which the waves did not lap onto the shore. However, in areas with wet concrete, issues similar to those for riprap revetments occurred (upper corner of Fig. 16(c)); some wet concrete surfaces were identified as water surfaces because of the similarity in panchromatic intensity between these surfaces. Occasionally, an entire section of the vertical structure area was missing (upper corner of Fig. 16(c)), resulting in extensive shoreline delineation errors. Breaking waves along the areas with vertical structures may also create shoreline delineation errors (lower corner of Fig. 16(c)). Examination of the bluff areas (center of Fig. 16(d)) indicated a significantly higher delineation error than that of sloped structure areas; this high error was induced by the inaccurate classification of the water surface and the sediment bank below the bluff. Specifically, the sediment bank below the bluff in this area is typically piled with building materials and rocks that fall from the bluff top under the influence of heavy bluff erosion, thus resulting in the inaccurate classification. Most of the shadow problems created by individual trees were resolved, but tree clusters or forests could only be partially corrected (center of Fig. 16(e)). The delineated shoreline along the pier areas exhibited a high degree of error because anchored vessels were classified as man-made objects (Fig. 16(f)).

V. CONCLUSION

We developed a new shoreline delineation approach from an

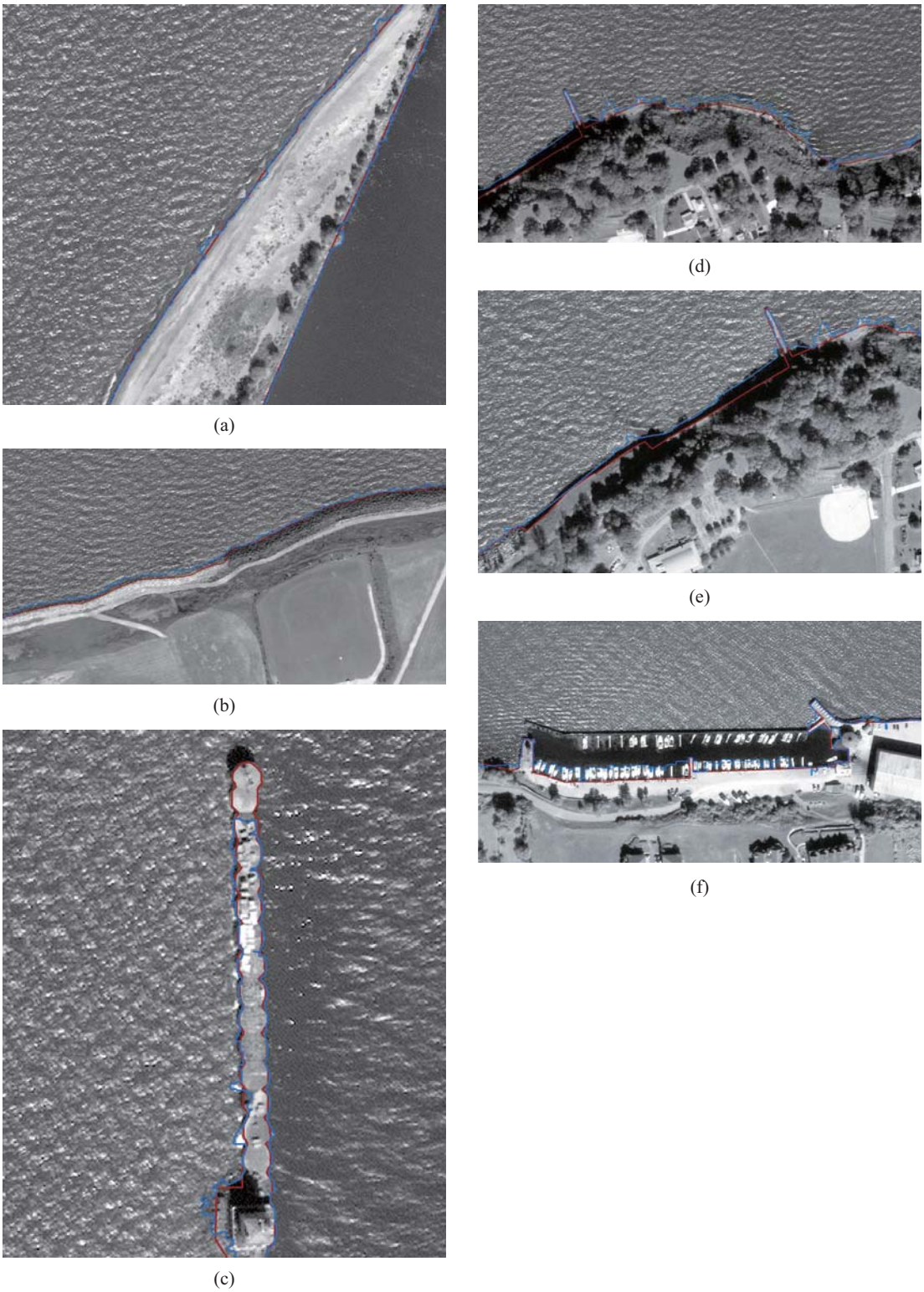

Fig. 16. Example of the shoreline delineated (blue line, ground truth shoreline in red) along (a) sediment bank areas, (b) sloped structure areas (riprap revetment areas), (c) vertical structure areas, (d) bluff areas, (e) shadow areas, and (f) pier areas.

object-oriented perspective that incorporates relatively low-cost data sources and reduces human labor while maintaining reasonable shoreline accuracy levels. The proposed approach extracts shorelines solely from WorldView-2 satellite imagery by applying spectral and shadow analysis to classify objects and terrain types. The use of shadow effects to analyze terrain

topography for image classification in order to delineate the shoreline from classification results is a new concept. The delineation results reveal that the extracted shoreline could reach an accuracy of 1.8 m (RMSE).

This shoreline delineation approach performed favorably with sediment banks, vertical structures, and groin areas. The accuracy level for piers was lowest because the anchored vessels were classified as man-made structures. Moreover, the accuracy corresponding to breakwaters was relatively low in this experiment because breakwaters beaten by waves are usually wet concrete blocks and identifying them correctly as man-made structures in a satellite image is difficult.

The proposed procedure can be immediately applied to applications for which the accuracy requirement is above 2 m; however, for applications with accuracy concerns, this procedure requires further improvement. One of the goals of this research was to develop an autonomous procedure for delineating shorelines; however, it has not been realized to date. The pan-transferring of the classification results required a supervised classification procedure to determine the segmentation parameters. An automatic process for determining pan-transferring parameters would be a useful addition to the current procedure that would improve the level of autonomy. Moreover, the proposed procedure utilizes most of the information a WorldView-2 satellite image provides; hence, additional information is required for more accurate classification of satellite imagery—either spatially or spectrally—to improve the shoreline delineation accuracy. Therefore, incorporating ALS point cloud or hyperspectral images as data sources would useful for future shoreline extraction research.

The advantage of the proposed procedure is the use of object-oriented concepts for object classification and shoreline delineation. The classes determined through this procedure can be integrated with other data sources for more accurate classification. For example, LiDAR point clouds can be used to further determine man-made objects from the sediment bank/man-made object class. Traditional supervised classification algorithms cannot easily incorporate vector or point cloud data along with a raster image. In this research, we provide a framework that is based on WorldView-2 satellite imagery for determining the boundary between water and land. This framework can easily incorporate other forms of data source to improve the classification results.

ACKNOWLEDGEMENTS

This research was for the most part completed during the author's Ph.D study at Ohio State University under the supervision of Dr. Rongxing Li, and it was funded by the Ohio Sea Grant College Program (R/CE-010). Special gratitude is extended to Dr. Fuan Tsai at National Central University for providing valuable perspectives and suggestions to improve this paper.

REFERENCES

Boak, E. H. and I. L. Turner (2005). Shoreline definition and detection: a review. Journal of Coastal Research, 688-703.

Comaniciu, D. and P. Meer (2002). Mean shift: A robust approach toward feature space analysis. Pattern Analysis and Machine Intelligence. IEEE Transactions on 24(5), 603-619.

Di, K., J. Wang, R. Ma and R. Li (2003). Automatic shoreline extraction from high-resolution Ikonos satellite imagery. Proceedings of the ASPRS 2003 Annual Conference, 5-9 May 2003, Anchorage, Alaska, unpaginated CD-ROM.

DigitalGlobe (2013). WorldView-2 Datasheet, URL: http://www.digitalglobe.com/downloads/WorldView2-DS-WV2-Web.pdf, (last date accessed: 25 December 2013).

Fukunaga, K. and L. Hostetler (1975). The estimation of the gradient of a density function, with applications in pattern recognition. Information Theory, IEEE Transactions on 21(1), 32-40.

Hicks, S. D. and P. Schureman (2000). Tide and current glossary, US Department of Commerce, National Oceanic and Atmospheric Administration, National Ocean Service, Silver Spring, Maryland, 33.

Ji, L., L. Zhang and B. Wylie (2009). Analysis of dynamic thresholds for the normalized difference water index. Journal of Photogrammetric Engineering and Remote Sensing 75(11), 1307-1317.

Lee, I.-C., B. Wu and R. Li (2009). Shoreline extraction from the integration of lidar point cloud data and aerial orthophotos using mean shift segmentation, Proceedings of the ASPRS 2009 Annual Conference, 9-13 March 2009, Baltimore, Maryland, unpaginated CD-ROM.

Leigh, G. E. (2012). Scope of work for shoreline mapping under the noaa coastal mapping program, US Department of Commerce, National Oceanic and Atmospheric Administration, National Ocean Service, National Geodetic Survey, Remote Sensing Division, Silver Spring, Maryland, 583.

Li, R., R. Ma and K. Di (2002). Digital tide-coordinated shoreline. Marine Geodesy 25(1-2), 27-36.

Li, R., K. Di and R. Ma (2003). 3-D shoreline extraction from IKONOS satellite imagery. Marine Geodesy 26(1-2), 107-115.

Liu, H. and K. Jezek (2004). Automated extraction of coastline from satellite imagery by integrating Canny edge detection and locally adaptive thresholding methods. International Journal of Remote Sensing 25(5), 937-958.

Liu, J.-K., R. Li, S. Deshpande, X. Niu and T.-Y. Shih (2009). Estimation of blufflines using topographic Lidar data and orthoimages. Journal of Photogrammetric Engineering and Remote Sensing 75(1), 69-79.

Padwick, C., M. Deskevich, F. Pacifici and S. Smallwood (2010). WorldView-2 pan-sharpening, Proceedings of the ASPRS 2010 Annual Conference, 26-30 April 2010, San Diego, California, unpaginated CD-ROM.

Robertson, W., D. Whitman, K. Zhang and S.P. Leatherman (2004). Mapping shoreline position using airborne laser altimetry. Journal of Coastal Research, 884-892.

Scott, J. W., L. R. Moore, W. Harris and M. D. Reed (2003). Using Landsat 7 Enhanced Thematic Mapper Tasseled Cap Transformation to extract shoreline. US Geological Survey Open-File Report OF 03, 272.

Sekovski, I., F. Stecchi, F. Mancini and L. Del Rio (2014). Image classification methods applied to shoreline extraction on very high-resolution multispectral imagery. International Journal of Remote Sensing 35(10), 3556-3578.

Shalowitz, A. (1964). Shore and Sea Boundaries; Vol. 2; Interpretation and use of Coast and Geodetic Survey data, US Dept. of Commerce, Coast and Geodetic Survey, 749.

Srivastava, A. (2005). A least-squares approach to improved shoreline modeling, Master thesis, The Ohio State University, Columbus, Ohio, 85.

Stockdon, H. F., A. H. Sallenger Jr., J. H. List and R. A. Holman (2002). Estimation of shoreline position and change using airborne topographic lidar data. Journal of Coastal Research, 502-513.

White, S. (2007). Utilization of LIDAR and NOAA's vertical datum transformation tool (VDatum) for shoreline delineation, Proceedings of the OCEANS 2007, 29 September-4 October 2007, Vancouver, BC, 1-6.

White, S. A., C. E. Parrish, B. R. Calder, S. Pe'eri and Y. Rzhanov (2011). Lidar-derived national shoreline: empirical and stochastic uncertainty analyses. Journal of Coastal Research, 62-74.

Yamazaki, F., W. Liu and M. Takasaki (2009). Characteristics of shadow and removal of its effects for remote sensing imagery. Proceedings of the Geoscience and Remote Sensing Symposium, 2009 IEEE International, IGARSS 2009, 2009, IV-426-IV-429.